Numerical simulation of low pressure die-casting aluminum wheel

*Mi Guofa[1], Liu Xiangyu[2], Wang Kuangfei[1], Fu Hengzhi[1]

(1. School of Materials Science and Engineering, Henan Polytechnic University, Jiaozuo 454003, P. R. China; 2. Department of Mechanical Engineering, Chengde Petroleum College, Chengde 067000, P. R. China)

Abstract: The FDM numerical simulation software, ViewCast system, was employed to simulate the low pressure die casting (LPDC) of an aluminum wheel. By analyzing the mold-filling and solidification stage of the LPDC process, the distribution of liquid fraction, temperature field and solidification pattern of castings were studied. The potential shrinkage defects were predicted to be formed at the rim/spoke junctions, which is in consistence with the X-ray detection result. The distribution pattern of the defects has also been studied. A solution towards reducing such defects has been presented. The cooling capacity of the mold was improved by installing water pipes both in the side mold and the top mold. Analysis on the shrinkage defects under forced cooling mode proved that adding the cooling system in the mold is an effective method for reduction of shrinkage defects.

Key words: numerical simulation; aluminum wheel; low pressure die casting; defect reduction; forced cooling

CLC number: TG146.2+1/TP391.9   Document code: A   Article ID: 1672-6421(2009)01-048-05

The automotive industry is moving towards expanding the application of light-weight aluminum alloy castings for various components that previously made from steels or cast irons, for example, more than 50% of new cars in North America are now equipped with aluminum alloy wheels [1]. Unfortunately, because of the multiple stringent requirements for surface finish, impact and fatigue performance, air tightness, geometric and rotational balance tolerances, aluminum alloy die-cast wheels are one of the most difficult castings to make in automotive and the rejection rates are often high compared with other aluminum castings [2].

Low-pressure die casting (LPDC) process is a near net shape casting method [3]. Due to the high precision and high efficiency requirements as well as its capacity for high quality wheels at low cost LPDC is considered as the dominant process for the production of aluminum alloy wheels. LPDC is a cyclic process, which begins with the pressurization of the furnace. The high pressure inside the furnace forces the aluminum melt to rise up and enter the die cavity where it solidifies by transferring the heat from the metal to the die. In LPDC process the melt is poured from the bottom of the mould, thus the mould-filling course is smooth and can be regulated easily. Meanwhile, castings are solidified under external

pressure, leading to compact components with roughly 10% improvement in their mechanical properties compared with those manufactured by conventional foundry techniques [4-8].

To reduce the cost, it is necessary to identify the hard-to-cast wheels prior to the die manufacture and prototyping, so that castability issues can be explored early in the designing stage to avoid the manufacture of faulty and expensive dies. To take such advantages, the die casting industry has now adopted the computer based simulation technique which showed advantages over the conventional trial-and-error methodologies for design and optimization [9-13]. In this paper, the numerical simulation system ViewCast was used to simulate the temperature and velocity fields during the filling and solidification stages of LPDC aluminum alloy wheel. The present work was aimed to predict the location and volume of defects, and modification has been applied to the original process in order to improve the quality of casting.

1 Experiment

1.1 Mathematical model

The flow of liquid metal was assumed to be incompressible Newtonian fluid and the governing equations at the LPDC filling and solidification stages are as follows:

Navier-stokes equation

$$\rho(\frac{\partial u}{\partial t} + u\frac{\partial u}{\partial x} + v\frac{\partial u}{\partial y} + w\frac{\partial u}{\partial z}) = -\frac{\partial p}{\partial x} + \rho g_x + \mu(\frac{\partial^2 u}{\partial x^2} + \frac{\partial^2 u}{\partial y^2} + \frac{\partial^2 u}{\partial z^2}) \quad (1)$$

$$\rho(\frac{\partial v}{\partial t} + u\frac{\partial v}{\partial x} + v\frac{\partial v}{\partial y} + w\frac{\partial v}{\partial z}) = -\frac{\partial p}{\partial y} + \rho g_y + \mu(\frac{\partial^2 v}{\partial x^2} + \frac{\partial^2 v}{\partial y^2} + \frac{\partial^2 v}{\partial z^2}) \quad (2)$$

$$\rho(\frac{\partial w}{\partial t} + u\frac{\partial w}{\partial x} + v\frac{\partial w}{\partial y} + w\frac{\partial w}{\partial z}) = -\frac{\partial p}{\partial z} + \rho g_z + \mu(\frac{\partial^2 w}{\partial x^2} + \frac{\partial^2 w}{\partial y^2} + \frac{\partial^2 w}{\partial z^2}) \quad (3)$$

*Mi Guofa

Male, born in 1966, professor, Ph.D, graduated from the Harbin Institute of Technology (HIT) in 1989 and majored in Foundry, and he got his master's degree and doctor's degree from HIT in 1992 and 1995, respectively. His research interests are mainly focus on metal solidification technology and new materials.
E-mail: peter@hpu.edu.cn

Continuity equation

$$\frac{\partial u}{\partial x}+\frac{\partial v}{\partial y}+\frac{\partial w}{\partial z}=0 \tag{4}$$

Heat-transfer equation

$$\rho C_p(\frac{\partial T}{\partial t}+u\frac{\partial T}{\partial x}+v\frac{\partial T}{\partial y}+w\frac{\partial T}{\partial z})=\lambda(\frac{\partial^2 T}{\partial x^2}+\frac{\partial^2 T}{\partial y^2}+\frac{\partial^2 T}{\partial z^2})+L\frac{\partial f_s}{\partial t} \tag{5}$$

Where ρ is the density; u, v and w, the velocity vectors; t, the time; μ, the dynamic viscosity of the liquid metal; g_x, g_y and g_z, the gravitational acceleration vectors; p, the pressure; C_p, the specific heat of molten metal; λ, the thermal conductivity; T, the temperature; L, the latent heat and f_s, the solid phase fraction at the solidification stage.

1.2 Geometric model

Figure 1 shows the geometric model of aluminum alloy wheel, which was imported into the ViewCast. It consists of 10,000,000 FDM meshes, as shown in Fig. 2. The step length of mesh generation was self-adjusting to ensure the thinnest part of the casting can be divided into three meshes and ensure the accuracy of flow simulation.

Fig. 1 3D model of aluminum alloy wheel

Fig. 2 The mesh of aluminum alloy wheel

1.3 Initial and boundary conditions

The wheel was cast from Sr-modified A356 (Al-7%Si-0.3%Mg) alloy and the mold material was H13 steel. The properties of the alloy and mold were listed in Table 1 and Table 2, respectively.

The pressure boundary condition can only be used if the pressure at the gate is known. The pressure applied on the liquid surface in the crucible was known in advance and the pressure at the ingate can be calculated with the Bernoulli equation

$$\frac{(P_i-P_v)}{\rho}+\frac{(V_i^2-V_v^2)}{2}+gh=0 \tag{6}$$

Where V_i is the velocity of fluid at the ingate; P_i refers to the

Table 1 Material properties of A356

Material properties	Values
Density	2.485×10⁻³ (g/mm³, for solid)
	2.415×10⁻³ (g/mm³, for liquid)
Viscosity	2.96×10⁻³ (g/(mm •s))
Specific heat	0.963 (J/(g •°C))
Thermal conductivity	0.151 (W/(mm •°C))
Latent heat	389 (J/g)
Liquidus temp.	615 °C
Solidus temp.	555 °C
Gravity	9,800 (mm/ s²)

Table 2 Material properties of H13 steel

Material properties	Values
Density	7.8×10⁻³ (g/mm³)
Specific heat	0.422 (J/(g •°C))
Thermal conductivity	0.0287 (W/(mm •°C))

pressure of fluid at the ingate; V_v is velocity of fluid surface in the crucible; P_v is the vapor pressure above fluid; and h is the height of ingate above the reservoir.

If we assume that the fluid velocity is relatively low (i.e. the dynamic pressure is negligible) and that the volume of the metal reservoir is substantially larger than the volume of the casting (i.e. the height of fluid is constant), then the ingate pressure can be expressed as a function of the applied air pressure minus the hydrostatic head of molten metal.

$$P_i=P_v-\rho gh \tag{7}$$

Although we have assumed that the height of the fluid is constant during the filling of each casting, this is not true from one casting to the next. As molten metal is consumed, the volume of fluid in the crucible will be reduced progressively and the ingate height will increase. Therefore, in theory, the ingate height should be measured before every simulation, but in practice, it is not necessary because the fluid is driven by the increase rate of the applied pressure, rather than the absolute pressure. Since the rate of increase is constant during the filling process of the casting, the height of the riser-tube is irrelevant. Based on the above analysis, the effect of molten metal's reduction in the crucible was neglected and the calculated pressure at the gate, at a pouring temperature of 700℃ and a mold temperature of 300℃, is listed in Fig. 3.
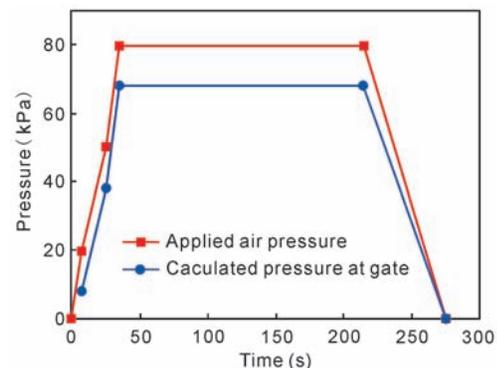

Fig. 3 The LPDC pressure curve

2 Simulation results and discussion

The mold-filling analysis was conducted on an aluminum wheel produced by the LPDC process, and the simulation results are shown in Fig. 4. It indicates the positions of the molten aluminum front in the cavity at different filling time. The whole filling process takes 16.9 s.
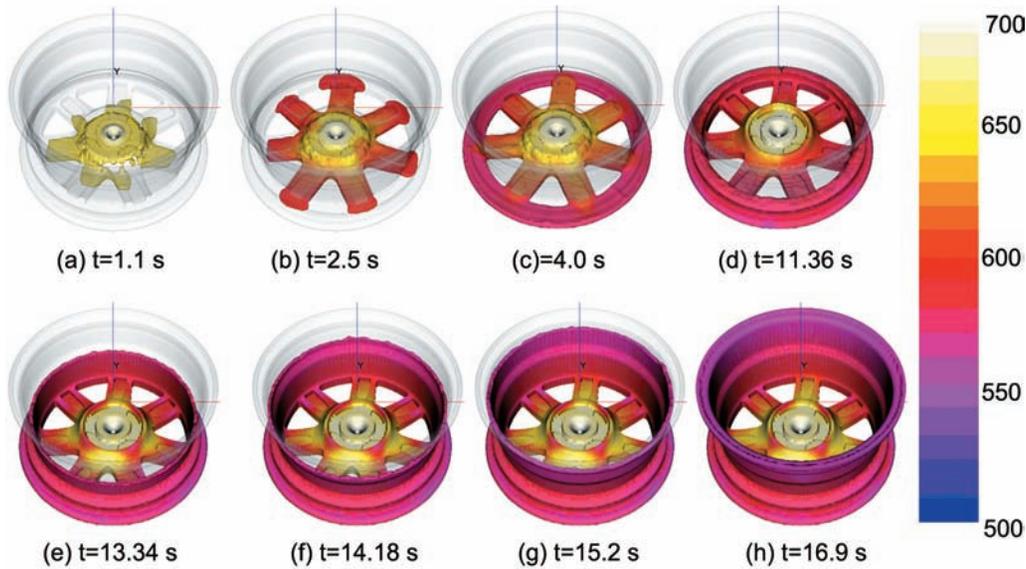

Fig. 4 Temperature distribution during mold-filling stage

At 1.1 s, the molten metal flows through the running system into the die cavity and then fills the centre of the hub. At 2.5 s, the front reaches the junctions between the rim and the spokes, and fills the bottom of the rim at 4 s. At this moment, the temperature of the alloy is about 600℃. The liquid metal reaches the middle of the rim at 13.34 s with a temperature of about 590℃, and reaches the top of the rim at 16.9 s. Figure 4 shows that the filling behavior is stable and propitious to prevent the formation of gas entrapment during the filling stage. When the cavity is filled entirely, no misrun and cold-shut are found at the top of the rim. At this time, the temperature of the front metal is about 580℃, which is in the semisolid state. In order to measure the temperature difference between the top and the bottom of the rim, three monitors were fixed at the middle of the rim, at the rim/spoke junction and at the top of the rim, respectively, as shown in Fig. 5. Figure 6 reveals the temperature evolution during the filling stage at these positions.
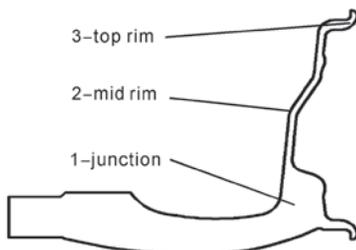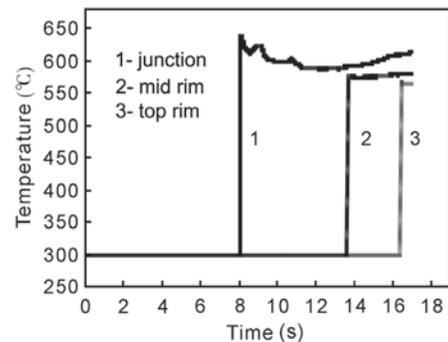

Fig. 6 Temperature curves of the monitored points during filling

Once the mold cavity is completely filled, solidification simulation is followed. The filling simulation results should be used as the initial temperature distribution of the solidification simulation for accuracy. Solidification is completed at 192 s. Figure 7 shows the solidification time at critical regions.

Figures 7(f) and (g) shown that solidification at the spokes, which begins at 53 s and finishes at 59 s, is faster than that at other positions. As a result, some isolated liquid regions (liquid islands) form at the rim/spoke junctions and eventually leading to shrinkages, as shown in Fig. 8. Figure 9 is the result of X-ray detection, exhibiting good agreement between the simulation and the practical measurement, with high accuracy for the predicted volume and position of the shrinkage.

During solidification stage, the temperature at the rim/spoke junction is higher than that at the middle rim and top rim, as shown in Fig. 10. Consequently, hot spots (liquid islands) at the rim/spoke junctions result (Fig. 7g), leading to potential shrinkages at the final stage of the solidification. Due to
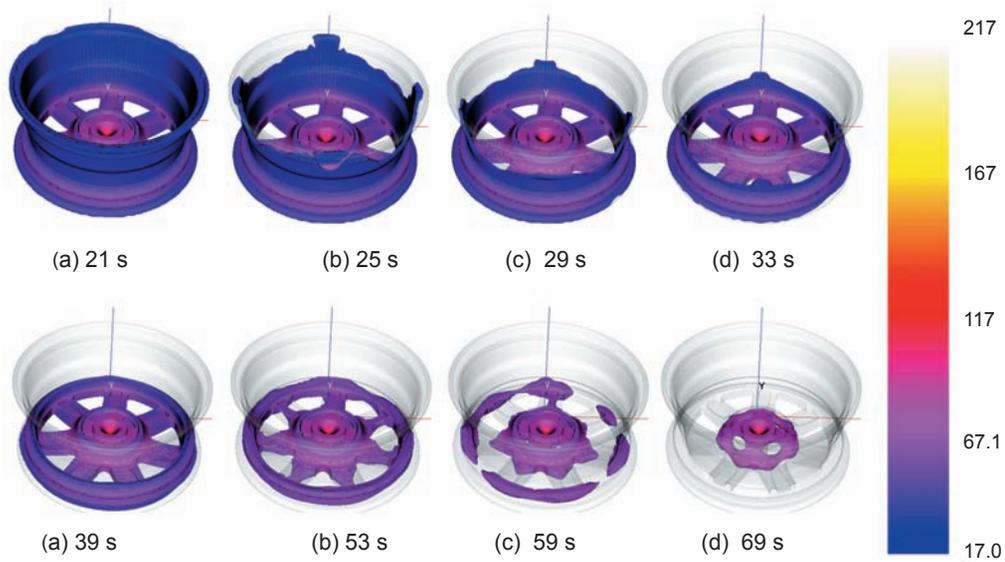

Fig. 5 Positions of monitors

(a) 21 s   (b) 25 s   (c) 29 s   (d) 33 s

(a) 39 s   (b) 53 s   (c) 59 s   (d) 69 s

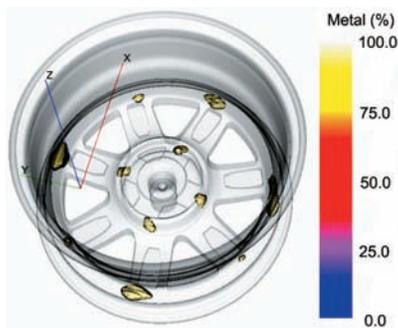**Fig. 7 Solidification time at critical regions**

Fig. 8 The predicted shrinkage defects
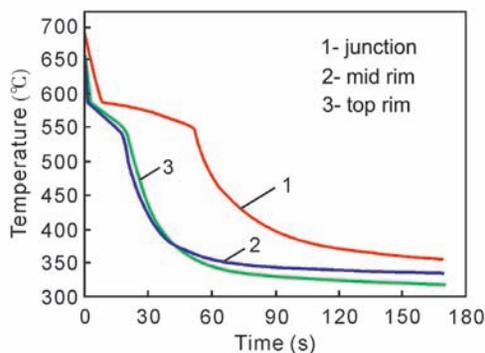

Fig. 9 Result of X-ray detection

Fig. 10 Temperature curves of the monitored points during solidification

the above reasons, the entire solidification process is not a directional solidification pattern from the rim top towards the hub center.

3 Defects reduction

Above analysis suggests that the hot spots occur at the rim/spoke junctions. In order to prevent the formation of shrinkage defects, the cooling capacity of the mold was enhanced by adding cooling water pipes at both the top mold and the side mold, as shown in Fig. 11. The diameter of the water pipe is 20 mm, and the temperature of the cooling water is 20℃.
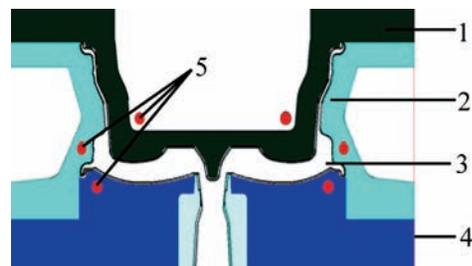
1-Top mold 2-Side mold 3-Casting
4-Lower mold 5-Water pipes

Fig. 11 Sketch showing the location of cooling water pipes

Figure 12 displays the solidification sequence of the wheel under forced-cooling. It showed that the time for the generation of liquid islands is about 44 s, which is brought forward by about 15 s when compared with the result obtained by using of the mold without forced-cooling. The liquid islands disappeared about 18 s ahead of the original process. In comparison of Fig. 7 with Fig. 12, it can be seen that the volume of the liquid island was decreased, however their locations remain unchanged. We shall study and optimize the process to shift the liquid islands in the center of the wheel in the future. Figure 13 shows the simulation result of defect under forced-cooling.
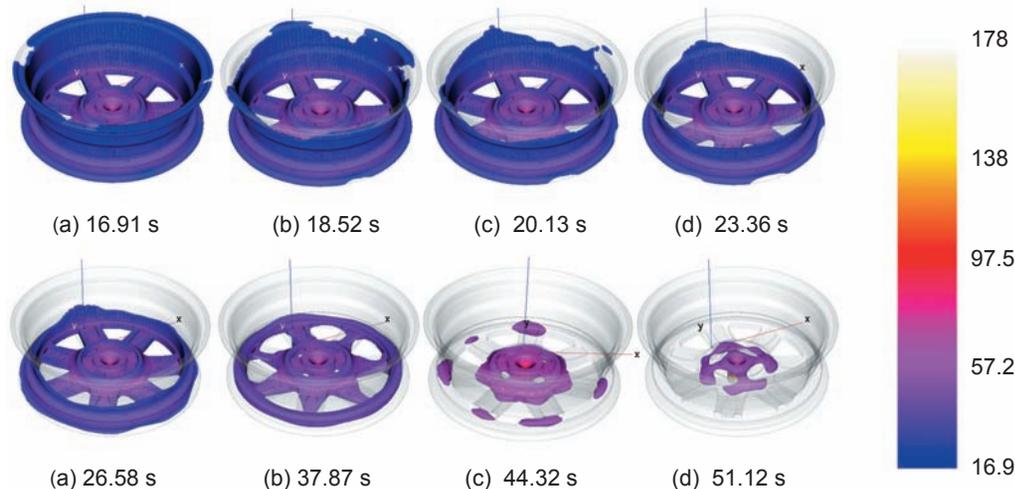
(a) 16.91 s	(b) 18.52 s	(c) 20.13 s	(d) 23.36 s

(a) 26.58 s	(b) 37.87 s	(c) 44.32 s	(d) 51.12 s

178
138
97.5
57.2
16.9

According to the above analysis, it seems that defects that caused by the structure of the casting can be reduced to a certain extent but cannot be totally eliminated. Defects are hard to be eliminated without structural modification of the casting. This is also in line with the actual results [14].

Fig. 12 Solidification time at critical regions under forced-cooling

Fig. 13 Predicted shrinkage defects under forced-cooling

4 Conclusions

Numerical simulation was applied to LPDC of aluminum wheel. The filling and solidification stages were numerically analyzed. Conclusions were drawn as the following:

(1) Study on positions of the molten front in the cavity at different filling time has revealed that the filling behavior of the LPDC process is stable, which is favorable for the prevention of gas entrapment at the filling stage, hence, avoid the formation of gas pores in the casting. The temperature field investigation indicate that the temperature distribution in this stage is appropriate, and there is no misrun and cold-shut formed at the top of the rim.

(2) The potential of forming shrinkage defects at the rim/spoke junctions was predicted, and the predicted result agrees well with the results obtained by X-ray detection analysis.

(3) Cooling water pipes in both of the side mold and the top mold can reduce the hot spots at rim/spoke junctions. This led to the decrease of the liquid island volume to a certain extent and satisfies the practical requirement in production.

References

[1] Chiesa F. Influence of some processes and metallurgical factors on production of cast Al wheels. *AFS Trans.*, 1995(103): 547–554.

[2] Zhang B, Cockcroft S L, Maijer D M, et al. Casting defects in low-pressure die-cast aluminum alloy wheels. *JOM*, 2005, 57(11): 36–43.

[3] Bonollo F, Urban J, Bonatto B, et al. Gravity and Low pressure die casting of aluminum alloys: A technical and economical benchmark. *Metallurgia Italiana*, 2005, 97(6): 23–32.

[4] Anon. Low pressure permanent mould casting of magnesium. Recent developments. *Foundry Trade Journal*, 1989, 163(3399): 3–7.

[5] Srinivasan A, Pillai U T S, John V, et al. Low-pressure casting of LM25 (Al-7Si-0.3 Mg) aluminum alloy. *Materials and Manufacturing Processes*, 2005, 20(2): 221–230.

[6] Plume A W. Low-pressure die casting - A practical assessment. *Foundry Trade Journal International*, 1982, 5 (16): 14–16, 18.

[7] Kreziak G, Rigaut C, Santarini M. Low pressure permanent mould process simulation of a thin wall aluminum casting. *Materials Science & Engineering A*: Structural Materials: Properties, Microstructure and Processing, 1993, A173 (1–2): 255–259.

[8] Wang Tao, Ma Zhiyi, Zhang Ye, et al. Simulation of low pressure casting process for thin-wall magnesium alloy casting. *Foundry*, 2004, 53 (5): 396–398. (in Chinese)

[9] Wang Li, Yang Yi, Luo Peng. Numerical simulation technology of high/low pressure die casting and its application. *Foundry Technology*, 2004, 25(3): 182–183. (in Chinese)

[10] Xu Hong, Hou Hua, Yang Jing, et al. CAD/CAE technology of electromagnetic low pressure die casting for aluminum alloys. *Acta Armamentarii*, 2006, 27 (3):510–514. (in Chinese)

[11] Xu Zhian. Designing a Gating and Feeding System for Aluminum Casting by using a Computer Program. Conference Proceedings from Materials Solutions 2002, Advances in Aluminum Casting Technology II, Columbus, Oct. 7–9, 2002: 113–116.

[12] Liu Baicheng. Development trend of casting technique and computer simulation. *Foundry Technology*, 2005, 26 (7): 611–617. (in Chinese)

[13] Zhang B, Maijer D M, Cockcroft S L. Development of a 3-D thermal model of the low-pressure die casting (LPDC) process of A356 aluminum alloy wheels. *Material Science and Engineering A (2007)*, doi:10.1016/j.msea.2007.02.018.

[14] Avalle M, Belingardi G, Cavatorta M P, et al. Casting defects and fatigue strength of a die cast aluminium alloy: a comparison between standard specimens and production components. *International Journal of Fatigue*, 2002, 24 (1):1–9.